Sound reproduction systems using variable-directivity loudspeakers

M. A. Poletti[a)]
Industrial Research Ltd., P.O. Box 31-310, Lower Hutt, New Zealand

F. M. Fazi and P. A. Nelson
Institute of Sound and Vibration Research, University of Southampton, United Kingdom

(Received 22 April 2010; revised 23 November 2010; accepted 8 December 2010)

Sound reproduction systems using omnidirectional loudspeakers produce reflections from room surfaces which interfere with the desired sound field within the array. While active compensation systems can reduce the reverberant level, they require calibration in each room and are processor-intensive. Directional loudspeakers allow the direct to reverberant level to be improved within the array, but still produce a finite exterior field which reflects from the room surfaces. The use of variable-directivity loudspeakers allows the exterior field to be eliminated at low frequencies by implementing the Kirchhoff–Helmholtz integral equation. This paper investigates the performance of variable-directivity arrays in reducing reverberant levels and compares the results with those derived in a previous paper for fixed-directivity arrays. The results presented may have some impact on the design of commercial multi-channel systems for sound reproduction.
 [DOI: 10.1121/1.3533689]

PACS number(s): 43.60.Tj, 43.55.Jz, 43.38.Md, 43.60.Sx [WMC] Pages: 1429–1438

I. INTRODUCTION

Commercially available surround sound systems approximate two-dimensional (2D) sound reproduction using a relatively small number of loudspeakers in a circular array around a listener.[1,2] The use of a greater number of loudspeakers allows the holographic reproduction of wave fields over a larger volume of space using the 2D circular or three-dimensional (3D) spherical arrays.[3–17] The loudspeakers used in the current systems are typically omnidirectional at low frequencies and therefore, when used in typical listening rooms, produce early reflections and reverberation which add to the desired direct field produced within the array. The effects of the room can be reduced by acoustical treatment or by using active compensation systems which measure various directional responses at the desired listener position and then pre-compensate the loudspeaker signals to eliminate the room effects.[18–25]

A simpler reduction of room effects is possible by using directional loudspeakers which increase the level of direct sound relative to the reverberant field.[26,27] In Ref. 26, the use of fixed-directivity loudspeakers in 3D sound reproduction systems has been studied, and it has been shown that the use of hyper-cardioid loudspeakers improves the direct to reverberant sound ratio by a factor approaching 4, which accords with the characteristics of a single hyper-cardioid loudspeaker.[28,29]

A greater reduction of room effects is possible using an array of variable-directivity loudspeakers. These can be configured to reduce the exterior sound from the array using the Kirchhoff–Helmholtz (K–H) integral formula.[9–13,30–32] The K–H integral states that a desired sound field can be created in a volume of space with boundary S using monopole sources and dipole sources normal to the surface S and that the sound field outside that region is zero. The dipole and monopole amplitudes differ for each loudspeaker, and hence the K–H integral can be implemented using first-order variable-directivity loudspeakers.

This paper considers sound reproduction using variable-directivity approaches based on the K–H integral. A spherical loudspeaker array is assumed, and so the loudspeaker first-order responses are a weighted combination of a monopole and a radially oriented dipole response. We show that a mode-truncated solution produces superior results to a solution based on the direct discretization of the K–H integral,[33] and we also develop a mode-matching solution and compare it with the mode-truncated solution. Finally, we evaluate variable-directivity solutions by numerical simulations and compare the results with the fixed-directivity results derived in Ref. 26.

The theory in this paper follows in an analogous manner to that presented in Ref. 26 and we therefore briefly review the relevant results from Ref. 26 and then extend it to the variable-directivity case.

II. SPHERICAL HARMONIC DESCRIPTION OF SOUND FIELDS

Consider a sphere Ω_{r_L} of radius r_L centered on the origin. A sound field is referred to as an *interior* field if it satisfies the homogeneous wave equation in the interior of Ω_{r_L} and as an *exterior* field if it satisfies the homogeneous wave equation in the exterior of Ω_{r_L}.[30]

The solution of the wave equation can be expressed in spherical coordinates $\vec{r} = (r, \theta, \phi)$, where the arrow denotes a vector quantity, the vector norm $r = \|\vec{r}\|$ is the radial distance from the origin, θ is the elevation angle from the

a)Author to whom correspondence should be addressed. Electronic mail: m.poletti@irl.cri.nz

vertical z-axis, and ϕ is the azimuthal angle from the x-axis.[30] Assuming a harmonic time dependence of $\exp(-i\omega t)$, the spherical harmonic expansions of an interior and exterior sound field at angular frequency ω are

$$p(r,\theta,\phi,k)=\begin{cases}\sum_{n=0}^{\infty}\sum_{m=-n}^{n} j_n(kr)A_n^m(k)Y_n^m(\theta,\phi), & r<r_L\\ \sum_{n=0}^{\infty}\sum_{m=-n}^{n} h_n(kr)C_n^m(k)Y_n^m(\theta,\phi), & r>r_L\end{cases}, \tag{1}$$

where $k=\omega/c$ is the wave number, c is the speed of sound in meters per second (assumed to be uniform in $\mathbb{R}^3$), $A_n^m(k)$ and $C_n^m(k)$ are the expansion coefficients, $j_n(x)$ is the nth order spherical Bessel function, and $h_n(x)=h_n^{(1)}(x)$ is the nth order spherical Hankel function of the first kind. The spherical harmonic $Y_n^m(\theta,\phi)$ is defined as[32]

$$Y_n^m(\theta,\phi)=\sqrt{\frac{(2n+1)}{4\pi}\frac{(n-|m|)!}{(n+|m|)!}}P_n^{|m|}(\cos\theta)e^{im\phi}, \tag{2}$$

where $P_n^{|m|}(\cdot)$ is the associated Legendre polynomial. The assumption is made that the operating frequency ω and hence the wave number k are fixed, and therefore the dependence of the sound field and other functions of ω or k is not written explicitly.

A. Monopole and dipole sources

The acoustic pressure field generated by an ideal monopole source in the free field is of the form[30]

$$p_m(\vec{r},\vec{r}_s)=G(\vec{r}|\vec{r}_s)=\frac{e^{ik|\vec{r}-\vec{r}_s|}}{4\pi|\vec{r}-\vec{r}_s|}, \tag{3}$$

which has a spherical harmonic expansion

$$p_m(\vec{r},\vec{r}_s)=\begin{cases}ik\sum_{n=0}^{\infty}j_n(kr)h_n(kr_s)\sum_{m=-n}^{n}Y_n^m(\theta,\phi)Y_n^m(\theta_s,\phi_s)^*, & r<r_s\\ ik\sum_{n=0}^{\infty}j_n(kr_s)h_n(kr)\sum_{m=-n}^{n}Y_n^m(\theta,\phi)Y_n^m(\theta_s,\phi_s)^*, & r>r_s\end{cases}, \tag{4}$$

where $r=\|\vec{r}\|$ and $r_s=\|\vec{r}_s\|$.

A dipole at position $\vec{r}_s$ and oriented in direction $\vec{v}$ has a field that takes the form[31]

$$p_d(\vec{r},\vec{r}_s)=\frac{\partial G(\vec{r}|\vec{r}_s)}{\partial\vec{v}}=-ik\frac{e^{ik|\vec{r}-\vec{r}_s|}}{4\pi|\vec{r}-\vec{r}_s|}\left[1+\frac{i}{k|\vec{r}-\vec{r}_s|}\right]\cos\gamma, \tag{5}$$

where γ is the angle between $\vec{v}$ and $\vec{r}-\vec{r}_s$. As in Ref. 26, we equalize the dipole response by dividing by ik to produce a first-order directivity that is approximately independent of frequency. At a given distance r_d from the dipole source, the equalized response is flat for frequencies down to the transition frequency $f_d=c/(2\pi r_d)$ and rises at 6 dB per octave below that. Hence, to ensure flat responses down to a frequency f_d, we must maintain a distance from any equalized dipole greater than r_d.

The spherical harmonic expansion for a $1/(ik)$-equalized dipole oriented radially with respect to the origin is obtained from the derivative of Eq. (4) with respect to r_s

$$p_d(r,\theta,\phi)=\begin{cases}k\sum_{n=0}^{\infty}\sum_{m=-n}^{n}j_n(kr)h_n'(kr_s)Y_n^m(\theta,\phi)Y_n^m(\theta_s,\phi_s)^*, & r<r_s\\ k\sum_{n=0}^{\infty}\sum_{m=-n}^{n}j_n'(kr_s)h_n(kr)Y_n^m(\theta,\phi)Y_n^m(\theta_s,\phi_s)^*, & r>r_s\end{cases}, \tag{6}$$

where $j_n'(\cdot)$ and $h_n'(\cdot)$ are the derivatives of the corresponding spherical Bessel and Hankel functions.

B. Interior and exterior truncation error of monopole and dipole fields

If the series in Eqs. (4) and (6) are truncated to a given finite order, $n=N$, the representation of the field is no longer exact since it is affected by the so-called truncation error. In Ref. 26, the interior truncation error of the monopole and dipole are presented. For an evaluation of the exterior sound field produced by the array the exterior truncation error is also useful.

The angle-averaged normalized truncation error for a monopole with order N expansion $P_T(r,\theta,\phi)$ is defined as[6,8]

$$\bar{\varepsilon}_{TM}(N,kr)=\frac{\int_{\Omega_r}|p(r,\theta,\phi)-p_T(r,\theta,\phi)|^2d\Omega_r}{\int_{\Omega_r}|p(r,\theta,\phi)|^2d\Omega_r}, \tag{7}$$

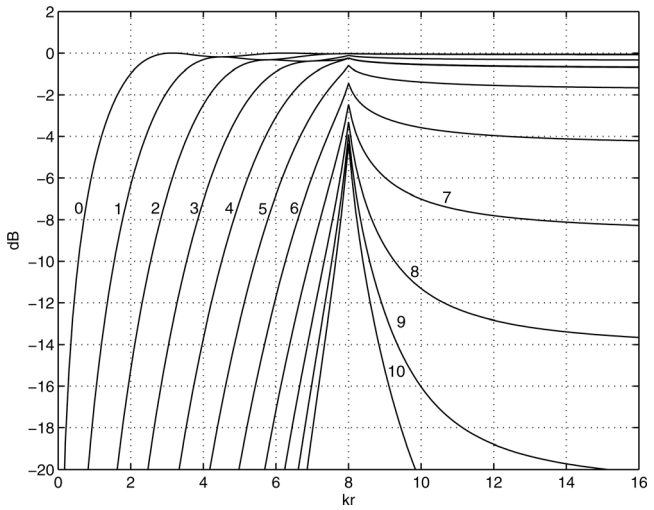

FIG. 1. Monopole truncation error for $kr_s = 8$ and orders $N = 0$ to 10.

where the overbar denotes an average over all angles. Substituting the monopole expansions, Eq. (4), yields the monopole truncation error

$$\bar{\varepsilon}_{TM}(N,kr) = \begin{cases} 1 - \dfrac{\sum_{n=0}^{N}(2n+1)j_n^2(kr)|h_n(kr_s)|^2}{\sum_{n=0}^{\infty}(2n+1)j_n^2(kr)|h_n(kr_s)|^2}, & kr < kr_s \\ 1 - \dfrac{\sum_{n=0}^{N}(2n+1)j_n^2(kr_s)|h_n(kr)|^2}{\sum_{n=0}^{\infty}(2n+1)j_n^2(kr_s)|h_n(kr)|^2}, & kr > kr_s\,. \end{cases} \tag{8}$$

The truncation error is shown for $kr_s = 8$ in Fig. 1. For $kr \ll kr_s$ the error is approximately -14 dB for $N \approx kr$.[6] For $k_r > kr_s$, the minimum order required to represent the exterior expansion at large kr is $N \approx kr_s$, where the asymptotic error again falls to around -14 dB or lower. However, if lower error is required, particularly for kr close to kr_s, then $N > kr_s$ is required.

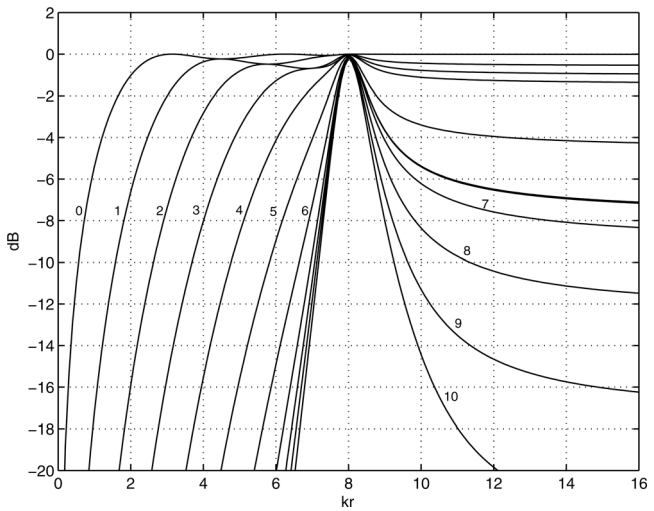

FIG. 2. Dipole truncation error for $kr_s = 8$ and orders $N = 0$ to 10.

The truncation error for the dipole is found from Eq. (6)

$$\bar{\varepsilon}_{TD}(N,kr) = \begin{cases} 1 - \dfrac{\sum_{n=0}^{N}(2n+1)j_n^2(kr)|h_n'(kr_s)|^2}{\sum_{n=0}^{\infty}(2n+1)j_n^2(kr)|h_n'(kr_s)|^2}, & kr < kr_s \\ 1 - \dfrac{\sum_{n=0}^{N}(2n+1)j_n'^2(kr_s)|h_n(kr)|^2}{\sum_{n=0}^{\infty}(2n+1)j_n'^2(kr_s)|h_n(kr)|^2}, & kr > kr_s\,. \end{cases} \tag{9}$$

This is shown in Fig. 2 for $kr_s = 8$. The error is around -16 dB for $N \approx kr$ and $kr \ll kr_s$ and for $kr > kr_s$, the error reduces asymptotically to around -12 dB for $N \approx kr_s$, 2 dB higher than the monopole case.

In summary, to represent accurately the exterior field due to a general first-order source, we require $N > kr_s$. For the interior representation of the source, $N = kr$ is sufficient, implying that low orders are sufficient for small radii.[26] Finally, for better accuracy near the source, orders higher than kr_s are required.

C. Loudspeaker array geometry and Nyquist frequencies

We will assume a spherical array of loudspeakers, each of which can produce ideal monopole and dipole fields, arranged at positions (r_L, θ_l, ϕ_l), $l \in [1, L]$, which approximate a uniform sampling over the sphere, with numerical weighting coefficients β_l, required for accurate numerical integration. A measure of the uniformity of the loudspeaker arrangement is given by the discrete cross-correlation of the spherical harmonics at the loudspeaker angles

$$\Gamma((n_1,m_1),(n_2,m_2)) = \sum_{l=1}^{L} \beta_l Y_{n_1}^{m_1}(\theta_l,\phi_l) Y_{n_2}^{m_2}(\theta_l,\phi_l)^*. \tag{10}$$

This matrix indicates the degree of orthonormality of the sampled spherical harmonics for the transducer arrangement adopted. In the ideal case of perfect orthonormality, the cross-correlation equals $\delta_{n_1 n_2}\delta_{m_1 m_2}$, where δ_{nm} is the Kronecker delta.[26] In practice at high orders, the sampled spherical harmonics are not orthogonal and this will contribute to reproduction errors at high frequencies.[26] The array is able to reproduce a sound field at a given wave number k and at radius r for $N > kr$ and hence [since there are $(N+1)^2$ spherical harmonics of order N] if $L \geq (\lceil kr \rceil + 1)^2$ uniformly arranged loudspeakers are used (see Ref. 6). This defines approximately the interior Nyquist frequency of the array[26]

$$f_{NI}(r) = \frac{c(\sqrt{L}-1)}{2\pi r}. \tag{11}$$

For the control of the exterior field for $r > r_L$ Fig. 2 shows that we require $L \geq (\lceil kr_L \rceil + 1)^2$. Therefore, surround systems which attempt to control the exterior field are able to do so up to the fixed exterior Nyquist frequency

$$f_{NE} = \frac{c(\sqrt{L} - 1)}{2\pi r_L}. \tag{12}$$

Hence, the interior Nyquist frequency increases toward the origin due to the focusing of the individual sound fields and the exterior Nyquist frequency is fixed since the Nyquist constraint ensures that the correct exterior field is generated near the array.

III. SOUND REPRODUCTION SYSTEMS WITH VARIABLE-DIRECTIVITY LOUDSPEAKERS

We now consider the implementation of the K–H integral. As in Ref. 26, we assume a continuous distribution of monopole and radially oriented dipole speakers on the surface of a sphere Ω_{r_L} of radius r_L at positions $\vec{r}_v = (r_L, \theta_v, \phi_v)$, $\theta_v \in [0, \pi]$, and $\phi_v \in [0, 2\pi]$. The exterior field is zero, and we write the interior field expression as

$$p(\vec{r}) = \int_{\Omega_{r_L}} \left[\frac{\partial p(\vec{r}_v)}{\partial \vec{n}(\vec{r}_v)} G(\vec{r}|\vec{r}_v) - ikp(\vec{r}_v) \frac{1}{ik} \frac{\partial G(\vec{r}|\vec{r}_v)}{\partial \vec{n}(\vec{r}_v)} \right] d\Omega_{r_L}, \quad r < r_L, \tag{13}$$

where $p(\vec{r}_v)$ is the sound pressure on the boundary of the region Ω_{r_L}, $d\Omega_{r_L} = r_L^2 \sin(\theta_V)\, d\theta_V d\phi_V$ is an element of solid angle, and where we have explicitly included the ik equalization of the dipole.

A. Direct solution for a single point source

For the case where the sound field is due to a point source outside the region at $\vec{r}_s$, the monopole source amplitudes are, from Eq. (5),

$$\frac{\partial p(\vec{r})}{\partial n} = ik \frac{e^{ik|\vec{r}_s - \vec{r}|}}{4\pi|\vec{r}_s - \vec{r}|} \left[1 + \frac{i}{k|\vec{r}_s - \vec{r}|} \right] \cos \upsilon, \tag{14}$$

where v is the angle between the normal and r_s. The dipole source amplitudes are, from Eq. (3),

$$ikp(\vec{r}) = ik \frac{e^{ik|\vec{r}_s - \vec{r}|}}{4\pi|\vec{r}_s - \vec{r}|}. \tag{15}$$

In practice a discrete array is used, using L loudspeakers arranged at positions $\vec{r}_l = (r_L, \theta_l, \phi_l)$ on Ω_{R_L}. The sound field $\hat{p}(\vec{r})$ reproduced by a discrete array approximation of Eq. (13) can be represented by

$$\hat{p}(\vec{r}) = \sum_{l=1}^{L} \left[G(\vec{r}|\vec{r}_l)\, u_l + \frac{1}{ik} \frac{\partial G(\vec{r}|\vec{r}_l)}{\partial \vec{n}(\vec{r}_l)} v_l \right], \tag{16}$$

where u_l and v_l are the monopole and equalized dipole amplitudes, respectively.

As for the fixed-directivity case, the weights in Eq. (14) and (15) are calculated for each loudspeaker position and scaled by $r_L^2 \beta_l$ to produce discrete monopole weights u_l and dipole weights v_l.

B. Mode-truncated solution

Equations (1), (4), and (6) have spherical harmonic expansions of infinite order. When implementing the integral in Eq. (13) using a discrete array as in Eq. (16), aliasing will occur for those spherical harmonics which cannot be controlled with the loudspeaker array.[33] This aliasing can be reduced by using mode-truncated forms of the monopole and dipole amplitudes.[33] In view of Eqs. (1) and (13), the order-N truncated expansion for the monopole amplitude in Eq. (16) is

$$\hat{u}_l = kr_L^2 \beta_l \sum_{n=0}^{N} \sum_{m=-n}^{n} j_n'(kr_L) A_n^m(k) Y_n^m(\theta_l, \phi_l). \tag{17}$$

Including the minus sign in the dipole weight amplitudes, the mode-truncated expansion of the dipole amplitude is derived from Eqs. (1) and (13)

$$\hat{v}_l = -ikr_L^2 \beta_l \sum_{n=0}^{N} \sum_{m=-n}^{n} j_n(kr_L) A_n^m(k) Y_n^m(\theta_l, \phi_l). \tag{18}$$

Substituting these solutions into Eq. (16) shows that, below the Nyquist frequency, they produce the correct sound field Eq. (1) if the loudspeaker positions produce the ideal orthonormality conditions in Eq. (10).

For the case of a point source, we obtain the following expressions for the mode-truncated weights:

$$\hat{u}_l \approx i(kr_L)^2 \beta_l \sum_{n=0}^{N} \sum_{m=-n}^{n} j_n'(kr_L) h_n(kr_s) Y_n^m(\theta_s, \phi_s)^* Y_n^m(\theta_l, \phi_l) \tag{19}$$

and

$$\hat{v}_l \approx (kr_L)^2 \beta_l \sum_{n=0}^{N} \sum_{m=-n}^{n} j_n(kr_L) h_n(kr_s) Y_n^m(\theta_s, \phi_s)^* Y_n^m(\theta_l, \phi_l). \tag{20}$$

C. Mode-matching solution

As for the fixed-directivity case,[26] a mode-matching solution can be derived for variable-directivity sound reproduction systems. This allows some control of the effects of non-orthogonality of the array at high mode orders. We determine the loudspeaker weights required to synthesize the field due to a monopole source, while requiring the exterior sound field to be zero. For simplicity, we assume that the monopole source generating the target field is outside the loudspeaker array. We require the interior spherical harmonic expansions of the sum of sound fields due to the L loudspeakers, with monopole weights $\bar{u}_l$ [applied to Eq. (4) for position $\vec{r}_l = (r_L, \theta_l, \phi_l)$] and radial dipole weights $\bar{v}_l$, [applied to Eq. (6)] to equal the desired field expansion in Eq. (1). For each (n, m), this produces

$$k\sum_{l=1}^{L}\left[ih_n(kr_L)\bar{u}_l + h_n'(kr_L)\bar{v}_l\right]Y_n^m(\theta_l,\phi_l)^* = A_n^m,$$
$$n\in[0,N],\ \ m\in[-n,n]. \quad (21)$$

Similarly, since we require zero exterior field, the exterior mode-matching equations for radii greater than the loudspeaker radius $r>r_L$ are

$$k\sum_{l=1}^{L}\left[ij_n(kr_L)\bar{u}_l + j_n'(kr_L)\bar{v}_l\right]Y_n^m(\theta_l,\phi_l)^* = 0,$$
$$n\in[0,N],\ \ m\in[-n,n]. \quad (22)$$

We note that Eq. (17) and (18) satisfy these two equations assuming discrete orthonormality of the spherical harmonics, $\Gamma((n_1,m_1),(n_2,m_2)) = \delta_{n_1,n_2}\delta_{m_1,nm}$ [Eq. (10)].

Equations (21) and (22) can be written in matrix notation

$$\begin{bmatrix}\boldsymbol{\Psi}_{IM} & \boldsymbol{\Psi}_{ID}\\ \boldsymbol{\Psi}_{EM} & \boldsymbol{\Psi}_{ED}\end{bmatrix}\begin{bmatrix}\mathbf{u}\\ \mathbf{v}\end{bmatrix} = \boldsymbol{\Psi}\begin{bmatrix}\mathbf{u}\\ \mathbf{v}\end{bmatrix} = \begin{bmatrix}\mathbf{d}\\ \mathbf{0}\end{bmatrix}, \quad (23)$$

where $\boldsymbol{\Psi}_{IM}$ is a $K=(N+1)^2$ by L matrix of interior monopole terms $\Psi_{IM}(b,l) = ikh_n(kr_L)Y_n^m(\theta_l,\phi_l)^*$, where $b=n^2+n+m+1$, $\boldsymbol{\Psi}_{ID}$ is a $K\times L$ matrix of interior dipole terms $\Psi_{ID}(b,l) = kh_n'(kr_L)Y_n^m(\theta_l,\phi_l)^*$, $\mathbf{u}$ is an $L\times 1$ vector of monopole weights $\bar{u}_l$, and $\mathbf{v}$ is an $L\times 1$ vector of dipole weights $\bar{v}_l$. Similarly, $\boldsymbol{\Psi}_{EM}$ is a $K\times L$ matrix of exterior monopole terms $\Psi_{EM}(b,l) = ikj_n(kr_L)Y_n^m(\theta_l,\phi_l)^*$ and $\boldsymbol{\Psi}_{ED}$ is a $K\times L$ matrix of exterior dipole terms $\Psi_{ED}(b,l) = kj_n'(kr_L)Y_n^m(\theta_l,\phi_l)^*$. Finally, $\mathbf{d}$ is a $K\times 1$ vector of desired sound field terms $d_b = A_n^m$ and $\mathbf{0}$ is a $K\times 1$ vector of zeros.

For $K\geq L$, the least squares solution to Eq. (23) is[35]

$$\begin{bmatrix}\mathbf{u}\\ \mathbf{v}\end{bmatrix} = \left[\boldsymbol{\Psi}^H\boldsymbol{\Psi}+\lambda_V\mathbf{I}\right]^{-1}\boldsymbol{\Psi}^H\begin{bmatrix}\mathbf{d}\\ \mathbf{0}\end{bmatrix}, \quad (24)$$

where λ_V is a regularization parameter and the superscript H denotes the conjugate transpose. For $K<L$, the minimum energy solution is[36]

$$\begin{bmatrix}\mathbf{u}\\ \mathbf{v}\end{bmatrix} = \boldsymbol{\Psi}^H\left[\boldsymbol{\Psi}\boldsymbol{\Psi}^H+\lambda_V\mathbf{I}\right]^{-1}\begin{bmatrix}\mathbf{d}\\ \mathbf{0}\end{bmatrix}. \quad (25)$$

D. Comparison of solutions

The matrix $\boldsymbol{\Psi}$ in Eq. (23) can be decomposed into the product of 2×2 block matrices

$$\boldsymbol{\Psi} = k\begin{bmatrix}i\mathbf{H} & \mathbf{H}'\\ i\mathbf{J} & \mathbf{J}'\end{bmatrix}\begin{bmatrix}\mathbf{Y} & \mathbf{0}\\ \mathbf{0} & \mathbf{Y}\end{bmatrix} = k\boldsymbol{\Phi}\mathbf{Y}_2, \quad (26)$$

where $\mathbf{H}$ and $\mathbf{H}'$ are the diagonal matrices whose terms are spherical Hankel functions and their first derivative, respectively, and analogously $\mathbf{J}$ and $\mathbf{J}'$ are diagonal matrices with spherical Bessel functions and their derivative, respectively. Note that each of these matrices have $2n+1$ repeated terms for each value of n. $\mathbf{Y}$ is a $K\times L$ matrix of spherical harmonic terms $\mathbf{Y} = Y_n^m(\theta_l,\phi_l)^*$. Since $\boldsymbol{\Phi}$ is block diagonal, its inverse is a block diagonal matrix of 2×2 inverse matrices

$$\boldsymbol{\Phi}^{-1} = \begin{bmatrix}i\mathbf{H} & \mathbf{H}'\\ i\mathbf{J} & \mathbf{J}'\end{bmatrix}^{-1} = \begin{bmatrix}\Delta^{-1} & 0\\ 0 & \Delta^{-1}\end{bmatrix}\begin{bmatrix}\mathbf{J}' & -\mathbf{H}'\\ -i\mathbf{J} & i\mathbf{H}\end{bmatrix}, \quad (27)$$

where Δ is the diagonal determinant $\Delta = i[\mathbf{HJ}'-\mathbf{JH}']$, which has the Wronskian property[30]

$$\Delta = i[\mathbf{HJ}'-\mathbf{JH}'] = \frac{1}{(kr_L)^2}\mathbf{I} \quad (28)$$

and hence

$$\boldsymbol{\Phi}^{-1} = (kr_L)^2\begin{bmatrix}\mathbf{J}' & -\mathbf{H}'\\ -i\mathbf{J} & i\mathbf{H}\end{bmatrix}. \quad (29)$$

Therefore, the mode-matching matrix in Eq. (23) can be written

$$\begin{bmatrix}\mathbf{Y} & \mathbf{0}\\ \mathbf{0} & \mathbf{Y}\end{bmatrix}\begin{bmatrix}\mathbf{u}\\ \mathbf{v}\end{bmatrix} = kr_L^2\begin{bmatrix}\mathbf{J}' & -\mathbf{H}'\\ -i\mathbf{J} & i\mathbf{H}\end{bmatrix}\begin{bmatrix}\mathbf{d}\\ \mathbf{0}\end{bmatrix} = kr_L^2\begin{bmatrix}\mathbf{J}'\mathbf{d}\\ -i\mathbf{J}\mathbf{d}\end{bmatrix}. \quad (30)$$

The mode-matching solution can therefore be written in the alternative form

$$\begin{bmatrix}\mathbf{u}\\ \mathbf{v}\end{bmatrix} = \begin{cases} kr_L^2\left[\mathbf{Y}_2^H\mathbf{Y}_2+\lambda_V\right]^{-1}\mathbf{Y}_2^H\begin{bmatrix}\mathbf{J}'\mathbf{d}\\ -i\mathbf{J}\mathbf{d}\end{bmatrix}, & K\geq L\\ kr_L^2\mathbf{Y}_2^H\left[\mathbf{Y}_2\mathbf{Y}_2^H+\lambda_V\right]^{-1}\begin{bmatrix}\mathbf{J}'\mathbf{d}\\ -i\mathbf{J}\mathbf{d}\end{bmatrix}, & K<L. \end{cases} \quad (31)$$

Furthermore, the mode-truncated solutions in Eq. (17) and (18) can be written in matrix form as

$$\begin{bmatrix}\hat{\mathbf{u}}\\ \hat{\mathbf{v}}\end{bmatrix} = kr_L^2\mathbf{B}\begin{bmatrix}\mathbf{Y}^H & \mathbf{0}\\ \mathbf{0} & \mathbf{Y}^H\end{bmatrix}\begin{bmatrix}\mathbf{J}'\mathbf{d}\\ -i\mathbf{J}\mathbf{d}\end{bmatrix} = kr_L^2\mathbf{B}\mathbf{Y}_2^H\begin{bmatrix}\mathbf{J}'\mathbf{d}\\ -i\mathbf{J}\mathbf{d}\end{bmatrix}, \quad (32)$$

where $\mathbf{B}$ is an $L\times L$ diagonal matrix of weighting coefficients β_l. It is now clear from a comparison of Eq. (31) with Eq. (32) that the mode-matching solution contains an additional inverse matrix which compensates for the non-uniformity of the loudspeaker array geometry, whereas the mode-truncated solution assumes orthogonality of the sampled spherical harmonics in using the Hermitian transpose of $\mathbf{Y}_2$ to obtain the associated solution.[8]

E. Robustness

As discussed in Ref. 26, the sensitivity of the loudspeaker array to variations in the loudspeaker polar responses and errors in the array layout is approximately governed by the condition number of the $K\times L$ matrix $\boldsymbol{\Psi}_V$.[34] This matrix has a singular value decomposition $\boldsymbol{\Psi}_V = \mathbf{US}_K\mathbf{V}^H$, where $\mathbf{U}$ is a $K\times K$ unitary matrix, $\mathbf{S}_K$ is a $K\times L$ matrix containing (at full rank) K singular values $[\sigma_1,\sigma_2,\ldots,\sigma_K]$, and $\mathbf{V}$ is an $L\times L$ unitary matrix.[34] For $K<L$, the K squared singular values of $\boldsymbol{\Psi}_V$ are the eigenvalues of

$$\boldsymbol{\Psi}_V\boldsymbol{\Psi}_V^H = \mathbf{US}_K^2\mathbf{U}^H = \boldsymbol{\Phi}\mathbf{Y}_2\mathbf{Y}_2^H\boldsymbol{\Phi}^H \approx \boldsymbol{\Phi}\boldsymbol{\Phi}^H, \quad (33)$$

where the last term assumes that the matrix $\mathbf{Y}_2$ is close to unitary. Therefore, the condition number is

$$\kappa_V = \|\boldsymbol{\Psi}_V\|\left\|\boldsymbol{\Psi}_V^{-1}\right\| = \|\boldsymbol{\Phi}\|\left\|\boldsymbol{\Phi}^{-1}\right\|, \quad (34)$$

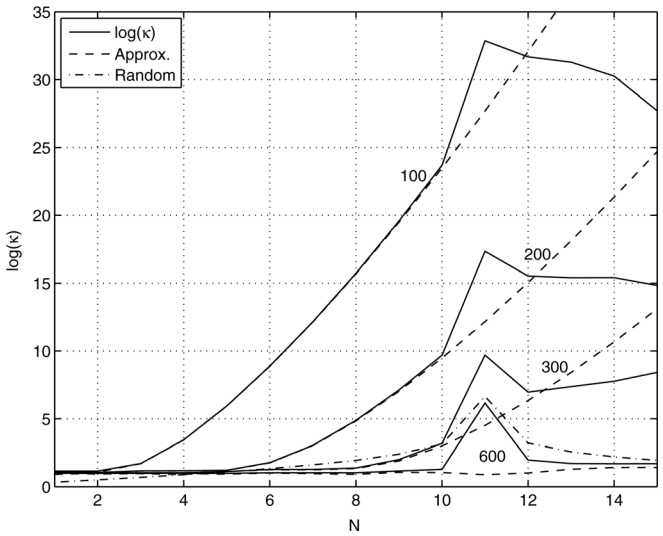

FIG. 3. Log(κ) at four frequencies from 100 to 600 Hz, $K=(N+1)^2<L$ approximation and random normal matrix result, $L=144$, $r_L=1.5$ m.

where $\|\bullet\|$ is the two-norm, equal to the largest singular value of $\mathbf{\Psi}_V$. The norm $\|\mathbf{\Phi}^{-1}\|$ is found from Eq. (29)

$$\left\|\mathbf{\Phi}^{-1}\right\| = (kr_L)^2 \left\| \begin{bmatrix} \mathbf{J}' & -\mathbf{H}' \\ -i\mathbf{J} & i\mathbf{H} \end{bmatrix} \right\| = (kr_L)^2 \|\mathbf{\Phi}\|, \tag{35}$$

since the adjugate matrix adj$\{\mathbf{\Phi}\}$ has the same singular values as $\mathbf{\Phi}$. Hence

$$\kappa_V = (kr_L)^2 \|\mathbf{\Phi}\|^2 = (kr_L)^2 \max\left\{eig\left\{\mathbf{\Phi}\mathbf{\Phi}^H\right\}\right\}. \tag{36}$$

Since $\mathbf{\Phi}$ is block diagonal, the eigenvalues of $\mathbf{\Phi}\mathbf{\Phi}^H$ are simply the (repeated) eigenvalues of the set of 2×2 matrices $\mathbf{\Phi}_2\mathbf{\Phi}_2^H$ where

$$\mathbf{\Phi}_2(n,kr_L) = \begin{bmatrix} ih_n(kr_L) & h_n'(kr_L) \\ ij_n(kr_L) & j_n'(kr_L) \end{bmatrix}, \quad n=0,N. \tag{37}$$

The largest eigenvalues occur for the maximum order $n=N$ and so

$$\kappa_V \approx (kr_L)^2 \max\{eig\{\mathbf{\Phi}_2(N,kr_L)\mathbf{\Phi}_2(N,kr_L)^H\}\}. \tag{38}$$

The condition number of $\mathbf{\Psi}$ is shown in Fig. 3 for four frequencies from 100 to 600 Hz. Equation (38) correctly predicts the condition number for $K<L$, when $K=L$ there is an increase in condition number, and Eq. (38) is not correct for $K>L$. At 600 Hz (above the Nyquist frequency), the conditioning becomes similar to that of the random matrix case, with a peak of $E\{\log(\kappa_V)\}=\log(2L)+0.982=6.64$.[37]

IV. SIMULATIONS

We now present simulations of sound fields produced by variable-directivity arrays in free-field conditions using the mode-truncated and mode-matched solutions. For comparison with the fixed-directivity case,[26] we also present simulations using arrays with weights given by

$$\hat{w}_l = \beta_l \sum_{n=0}^{N} \sum_{m=-n}^{n} \frac{A_n^m Y_n^m(\theta_l,\phi_l)}{k\left[aih_n(kr_L)+(1-a)h_n'(kr_L)\right]}, \quad l\in[1,L], \tag{39}$$

where a is a first-order weighting parameter which produces monopole loudspeaker responses for $a=1$ and dipole responses for $a=0$. With $a=0.25$, each loudspeaker polar response is a hyper-cardioid which produces the maximum direct to reverberant ratio in reverberant conditions.

We use a spherical array of 144 loudspeakers which are approximately uniformly arranged[34] at a radius of 1.5 m producing an exterior Nyquist frequency of 400 Hz. The near-field of the dipole responses occur at a radius r from the origin for which $k\,(r_L-r)=1$, which is a radius of 1.22 m at 200 Hz. Due to the poor conditioning of the mode-matching for the maximum possible mode order of 11 (see Fig. 3) and the need to maintain a high order for exterior control, we will use $N=10$ in the simulations. In this case, the mode-matched solution is given by Eq. (25) and the approximate condition number in Eq. (38) is valid.

The desired field is that due to a point source positioned on the x-axis at $r_s=3$ m. The error performance was found to be similar for all source angles, due to the regular arrangement of the loudspeakers, and the fact that the source distance is larger than the loudspeaker radius (so that the source position never coincides with a loudspeaker position).

A. Reproduction error and exterior field level

To quantify the performance of the solutions inside the array, we calculate the angle-averaged (radial) relative error between the desired field $p(r,\theta,\phi,k)$ and the reproduced field $\hat{p}(r,\theta,\phi,k)$ at radius $r<r_L$ (Ref. 6)

$$\bar{\varepsilon}(kr) = \frac{\int_{\Omega_r} |p(r,\theta,\phi,k)-\hat{p}(r,\theta,\phi,k)|^2 d\Omega_r}{\int_{\Omega_r} |p(r,\theta,\phi,k)|^2 d\Omega_r}. \tag{40}$$

This may be determined for a point source with spherical harmonic expansion coefficients $A_n^m = ih_n(kr_s)Y_n^m(\theta_s,\phi_s)^*$ using the orthogonality properties of the spherical harmonic expansions in Eqs. (1), (4), and (6) yielding (using as an example the mode-matching coefficients $\bar{u}_l$ and $\bar{v}_l$)

$$\bar{\varepsilon}(kr) = \frac{4\pi \sum_{n=0}^{\infty} j_n^2(kr) \sum_{m=-n}^{n} \left| \sum_{l=1}^{L} \left(i\,\bar{u}_l h_n(kr_L) + \bar{v}_l h_n'(kr_L)\right) Y_n^m(\theta_l,\phi_l)^* - ih_n(kr_s) Y_n^m(\theta_s,\phi_s)^* \right|^2}{\sum_{n=0}^{\infty} (2n+1) j_n^2(kr) |h_n(kr_s)|^2}. \tag{41}$$

To determine the performance of the surround system outside the array we calculate the angle-averaged exterior sound pressure magnitude squared, relative to the angle-averaged desired sound pressure magnitude squared at the loudspeaker radius

$$\bar{\Upsilon}(kr) = \frac{\int_{\Omega_r} |\hat{p}(r,\theta,\phi,k)|^2 d\Omega_r}{\int_{\Omega_{r_L}} |p(r_L,\theta,\phi,k)|^2 d\Omega_{r_L}}, \quad r > r_L \tag{42}$$

which can be written in terms of the spherical harmonics for a point source field in the form

$$\bar{\Upsilon}(kr) = 4\pi \frac{\sum_{n=0}^{\infty} |h_n(kr)|^2 \sum_{m=-n}^{n} \left| \sum_{l=1}^{L} \left(i\,\bar{u}_l j_n(kr_L) + \bar{v}_l j_n'(kr_L) \right) Y_n^m(\theta_l,\phi_l)^* \right|^2}{\sum_{n=0}^{\infty} (2n+1) j_n^2(kr_L) |h_n(kr_s)|^2}. \tag{43}$$

Equations (41) and (43) may also be used with the mode-truncated K–H weights $\hat{u}_l$ and $\hat{v}_l$ in Eqs. (19) and (20). In practice, we use a finite maximum order of $n=25$ in Eqs. (41) and (43) which produced negligible truncation error.

B. Simulation results

We first demonstrate the improvement in accuracy obtained using the mode-truncated form of the K–H integral Eqs. (19) and (20) compared to the direct form Eqs. (14) and (15) (corresponding to infinite order expansion).[33] Figure 4 shows the interior error and exterior relative field for both solutions at 200 and 600 Hz. At low frequencies, the direct and mode-truncated results are essentially the same. At 600 Hz, the amplitudes of the high-order terms for $N>10$ are significant, hence the error is larger for the direct solution, with an error of -17 dB at $r=0$, compared to less than -80 dB for the truncated case. The exterior error is around 5 dB higher for the direct solution. We, therefore, consider only the mode-truncated and mode-matched solutions in the following simulations.

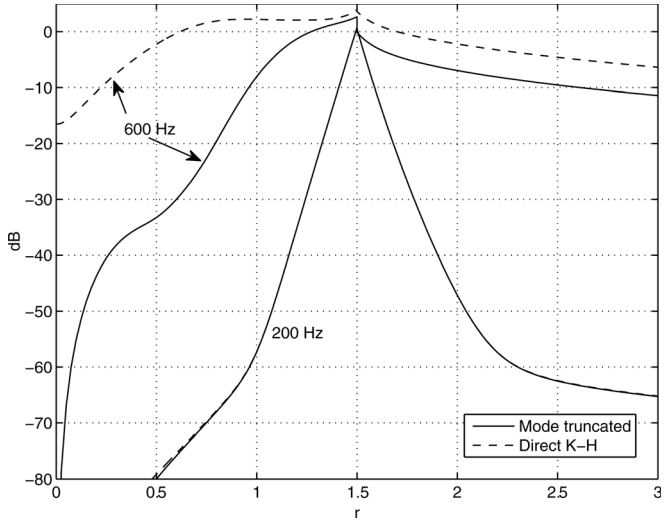

FIG. 4. Interior radial error ($r<1.5$ m) and relative exterior sound level ($r>1.5$ m) for direct and mode-truncated K–H solutions at 200 and 600 Hz.

Figures 5 and 6 show the real part of the sound fields (at $t=0$) obtained from the truncated-fixed solution with $a=0.25$ (hyper-cardioid) and the variable-directivity solution [Eqs. (19) and (20)]. (The corresponding mode-matched solution wave fields were similar in appearance, and their relative error performance is considered shortly.) The dashed circle indicates the loudspeaker radius and the dark circle is the maximum radius $r_N = \left(\sqrt{L}-1\right)/k$ where the mode-limited reproduction can maintain accuracy. The sound field produced by the fixed-directivity solution propagates across the interior of the array and beyond it. In contrast, the energy of the variable-directivity field is largely confined to the interior of the array and the exterior field is very small. This is shown more clearly by the radial error, shown in Fig. 7. Mode-truncated and mode-matched results are shown for both fixed- and variable-directivity cases, together with the

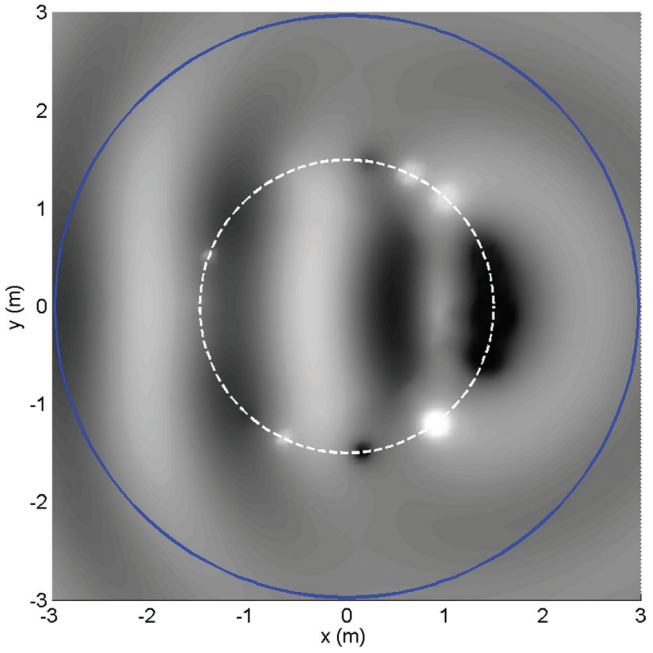

FIG. 5. (Color online) Fixed-directivity sound fields for $f=200$ Hz, $r_L=1.5$ m, $r_s=3$ m, and $a=0.25$.

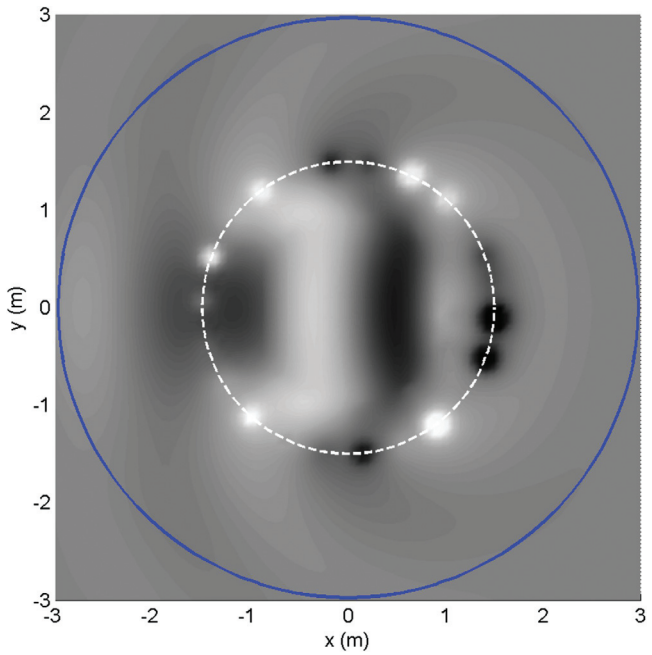

FIG. 6. (Color online) Variable-directivity sound fields for $f=200$ Hz, $r_L=1.5$ m, and $r_s=3$ m.

interior truncation error for the source [Eq. (8)], which represents the lowest possible error for a truncation limit of $N=10$. The mode-matching errors are shown for regularization parameters of $\lambda_V=0.0001$ and 0.001 to show how they vary with the regularization.

The interior errors are approximately the same for both the fixed- and the variable-directivity solutions, showing that there is no significant penalty associated with the exterior cancellation of the sound field. The mode-matching errors are approximately constant with radius near the center of the array. They are around -50 dB for $r<1$m for $\lambda_V=0.001$ and are about -70 dB for $\lambda_V=0.0001$. The mode-truncated solution errors reduce with radius and are below -80 dB at the center of the array.

The mode-matched solutions are able to provide a more consistent accuracy across a wider area than the mode-truncated solutions and can reduce the error at larger radii. Increasing the regularization raises the error floor (by around 20 dB in this example).

The variable-directivity relative exterior sound level falls to below -70 dB at $r=3$ m for the mode-matched solution with $\lambda_V=0.0001$, to below -50 dB for $\lambda_V=0.001$, and to around -65 dB for the mode-truncated case. These results are over 40 dB lower than the fixed-directivity exterior levels which both reduce to around -10 dB. Hence at low frequencies (below the exterior Nyquist frequency), the exterior field is significantly reduced by the variable-directivity array compared to the fixed-directivity array.

The truncation error for the monopole source is also shown in Fig. 7. It is below -80 dB for radii less than 1 m. The reproduced sound fields do not approach this lower limit since all positions greater than $r=0.27$ m are in the near-field of the loudspeakers, where the truncation error for the loudspeaker sources is large (Figs. 1 and 2).

Figures 8 and 9 show the fixed-directivity and variable-directivity mode-truncated sound fields produced at 600 Hz, above the exterior Nyquist frequency of the array (400 Hz). In both cases, the interior field is accurate to a radius $r_N=1$ m. Both arrays now produce an appreciable exterior field. The variable-directivity field is smaller in the direction toward the source (at $x=3$ m) and on the downstream side of the array from the source but produces larger radiation in lateral directions. The fixed-directivity solution does not reduce the downstream propagation, and the sound wave propagates out of the array on the far side. There is also some lateral radiation of sound producing interference effects.

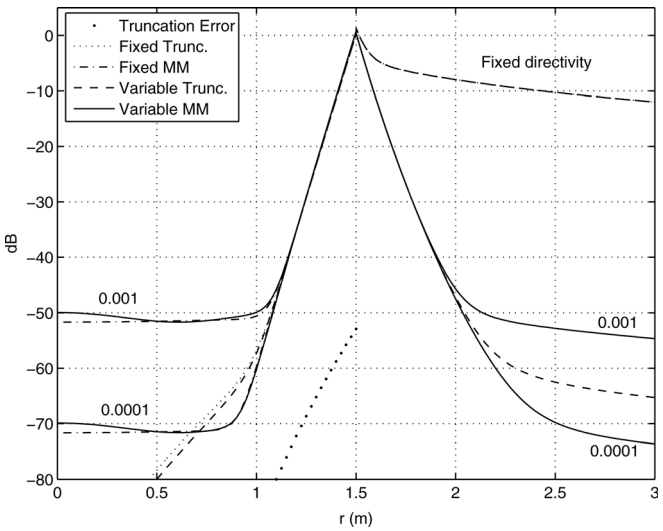

FIG. 7. Variable mode-truncated and mode-matched radial error ($r<1.5$ m), and relative exterior sound level ($r>1.5$ m) for $f=200$ Hz, $a=0.25$, $r_L=1.5$ m, $r_s=3$ m, and $N=10$, for regularization parameters of 0.001 and 0.0001. The fixed-directivity mode-truncated and mode-matched results and truncation error for $N=10$ and $r<1.5$ m are also shown for comparison.

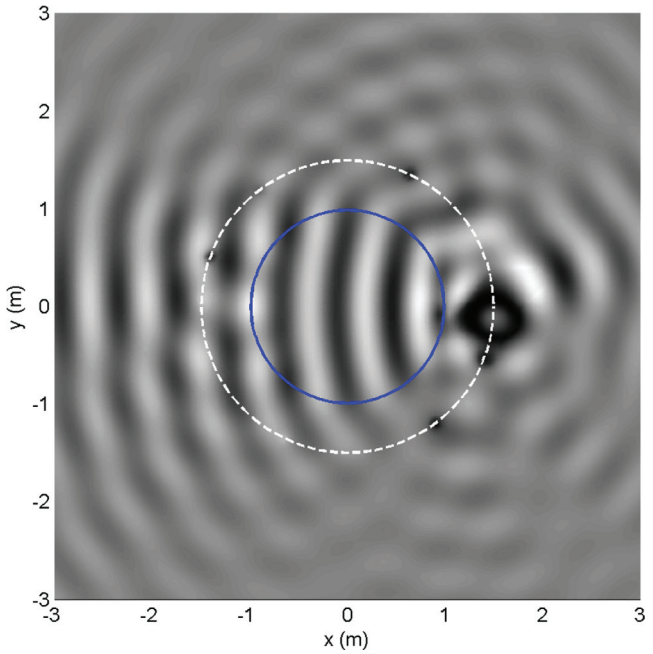

FIG. 8. (Color online) Fixed-directivity mode-truncated sound field for $f=600$ Hz, $r_L=1.5$ m, $r=3$ m, and $a=0.25$.

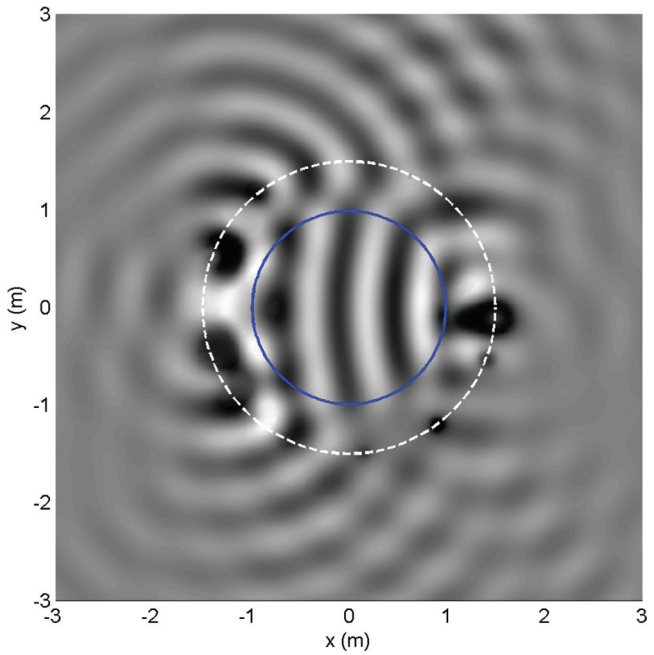

FIG. 9. (Color online) Variable-directivity mode-truncated sound fields for $f = 600$ Hz, $r_L = 1.5$ m, and $r_s = 3$ m.

The angle-averaged radial error is shown in Fig. 10. The interior sound fields produce an error close to the truncation limit, but the mode-match solutions are able to maintain accuracy down to $r = 0.5$ m, whereas the mode-truncated solutions diverge from the minimum error at $r = 0.8$ m. The exterior field levels produced by the variable-directivity solutions are now 2 dB higher than the fixed-directivity level and so the benefit of variable-directivity is lost.

At higher frequencies, the variable-directivity solution tends to produce radiation lobes at a variety of angles on the downstream side of the array, caused by the unsuccessful attempt to cancel the sound propagating from the interior of the array to its exterior. The fixed-directivity solution produces a simpler exterior field in the region opposite to the virtual source location, but a more significant backward radiation of sound toward the virtual source. Generally the fixed-directivity exterior sound level is slightly lower than the variable-directivity level, and so at frequencies above the exterior Nyquist frequency, a fixed-directivity solution is preferable.

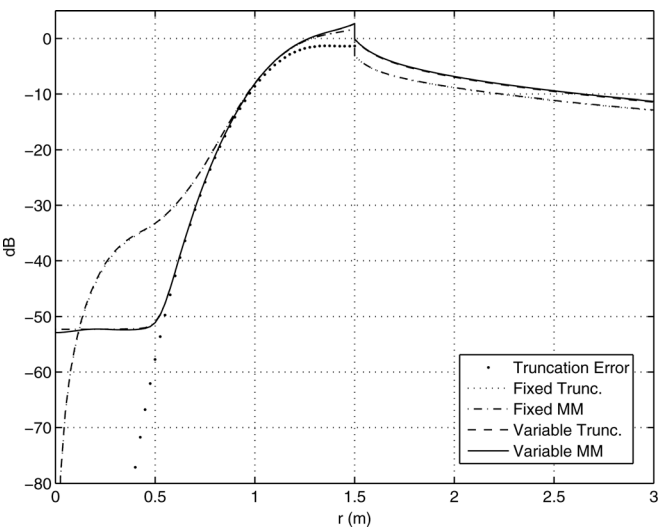

FIG. 10. Variable mode-truncated and mode-matched radial errors ($r < 1.5$ m) and relative exterior field ($r > 1.5$ m) for $f = 600$ Hz, $a = 0.25$, $r_L = 1.5$ m, $r_s = 3$ m, and $N = 10$. The fixed-directivity mode-truncated and mode-matched results and truncation error for $N = 10$ and $r < 1.5$ m are also shown for comparison.

V. CONCLUSIONS

This paper has investigated the production of three-dimensional sound fields using loudspeakers with variable-directivity with the goal of reducing the low-frequency reverberant field that occurs with sound reproduction in rooms. The exterior—and hence the reverberant—field can be eliminated below the exterior Nyquist frequency of the array with no appreciable increase in interior reconstruction error in comparison with fixed-directivity solutions. Above this frequency, the array cannot cancel the exterior field and fixed-directivity is more effective.

This paper has demonstrated that low-frequency control of room acoustics is possible in 3D surround systems without the need to take into account the modal behavior of the room. The sound system does not need to be calibrated *in-situ* and is therefore simpler than adaptive systems, but it does require first-order loudspeakers with variable-directivity which have closely matched polar responses. Furthermore, it does not eliminate sound scattered from the listener and reflected from the room surfaces.

We also note that the theory presented here is applicable to any practical situation where 3D wave fields are synthesized using an open sphere of directional transducers and that such an array avoids the modal resonances that would be produced by an array inside a solid enclosure (if the loudspeakers were arranged on a rigid wall). However, it does produce finite exterior fields above the exterior Nyquist frequency of the array.

The results in this paper are restricted to numerical simulations and we have not investigated practical variable-directivity loudspeakers, or the phase and amplitude matching performance of typical transducers. Since exterior cancellation is only possible at low frequencies, a practical loudspeaker product would provide monopole and dipole responses for the woofer (either as a number of fixed combinations for fixed-directivity applications or with discrete inputs for variable-directivity use) and the tweeter would produce a single response with the directivity governed by the loudspeaker baffle and tweeter diaphragm size. Such loudspeakers would also prove beneficial in stereo sound systems for reducing the effect of low-frequency modes. An alternative approach would be to use separate woofer and tweeter arrays, with a larger number of tweeters to extend the accurate region of the interior sound field and reduce the exterior field at higher frequencies.

ACKNOWLEDGMENTS

This work has been partially funded by the Royal Academy of Engineering and by the Engineering and Physical Sciences Research Council.

[1]M. A. Gerzon, "Ambisonics in multichannel broadcasting and video," J. Audio Eng. Soc. **33**(11), 859–871 (1985).
[2]M. A. Gerzon, "Optimum reproduction matrices for multispeaker stereo," J. Audio Eng. Soc. **40**(7/8), 571–589 (1992).
[3]M. Gerzon, "Periphony: With-height sound reproduction," J. Audio Eng. Soc. **21**(1), 2–10 (1973).
[4]O. Kirkeby and P. A. Nelson, "Reproduction of plane wave sound fields," J. Acoust. Soc. Am. **94**(5), 2992–3000 (1993).
[5]M. A. Poletti, "A unified theory of horizontal holographic sound systems," J. Audio Eng. Soc. **48**(12), 1155–1182 (2000).
[6]D. B. Ward and T. D. Abhayapala, "Reproduction of a plane-wave sound field using an array of loudspeakers," IEEE Trans. Speech, Audio Process. **9**(6), 697–707 (2001).
[7]J. Daniel, "Spatial sound encoding including near field effect: Introducing distance coding filters and a viable new ambisonics format," *in Proceedings of the 23rd International Conference of AES* (2003).
[8]M. A. Poletti, "Three-dimensional surround sound systems based on spherical harmonics," J. Audio Eng. Soc. **53**(11), 1004–1025 (2005).
[9]A. J. Berkhout, D. de Vries, and P. Vogel, "Acoustic control by wave field synthesis," J. Acoust. Soc. Am. **93**(5), 2764–2778 (1993).
[10]M. M. Boone, E. N. G. Verheijen, and P. F. Van Tol, "Spatial sound-field reproduction by wave-field synthesis," J. Audio Eng. Soc. **43**(12), 1003–1012 (1995).
[11]D. de Vries, "Sound reinforcement by wavefield synthesis: Adaptation of the synthesis operator to the loudspeaker directivity characteristics," J. Audio Eng. Soc. **44**(12), 1120–1131 (1996).
[12]S. Takane, Y. Suzuki, and T. Sone, "A new method for global sound field reproduction based on Kirchhoff's integral equation," Acust. Acta Acust. **85**, 250–257 (1999).
[13]S. Ise, "A principle of sound field control based on the Kirchhoff-Helmholtz integral equation and the theory of inverse systems," Acust. Acta Acust. **85**, 78–87 (1999).
[14]N. Epain and E. Friot, "Active control of sound inside a sphere via control of the acoustic pressure at the boundary surface," J. Sound Vib. **299**, 587–604 (2007).
[15]F. M. Fazi, P. A. Nelson, J. E. N. Christensen, and J. Seo, "Surround system based on three-dimensional sound field reconstruction," in *Proceedings of the 125th Convention of AES* (October 2–5, 2008).
[16]F. M. Fazi and P. A. Nelson, "A theoretical study of sound field reconstruction techniques," in *Proceedings of the 19th International Congress on Acoustics* (September 2–7, 2007).
[17]J. Ahrens and S. Spors, "An analytical approach to sound field reproduction using circular and spherical loudspeaker distributions," Acta Acust. Acust. **94**, 988–999 (2008).
[18]P. A. Nelson, F. Orduna-Bustamante, and H. Hamada, "Multi-channel signal processing techniques in the reproduction of sound," J. Audio Eng. Soc. **44**(11), 973–989 (1996).
[19]P. A. Nelson, H. Hamada, and S. J. Elliot, "Adaptive inverse filters for stereophonic sound reproduction," IEEE Trans. Signal Process. **40**(7), 1621–1632 (1992).
[20]T. Betlehemxy and T. Abhayapala, "Theory and design of sound field reproduction in reverberant rooms," J. Acoust. Soc. Am. **117**, 2100–2111 (2005).
[21]P.-A. Gauthier and A. Berry, "Adaptive wave field synthesis for sound field reproduction: Theory, experiments, and future perspectives," J. Audio Eng. Soc. **55**(12), 1107–1124 (2007).
[22]P.-A. Gauthier, A. Berry, and W. Woszczyk, "Sound-field reproduction in-room using optimal control techniques: Simulations in the frequency domain," J. Acoust. Soc. Am. **117**(2), 662–678 (2005).
[23]S. Spors, M. Renk, and R. Rabenstein, "Limiting effects of active room compensation using wave field synthesis," in *Proceedings of the 118th Convention of AES*, Barcelona, Spain (May 28–31, 2005).
[24]S. Spors, H. Buchner, R. Rabenstein, and W. Herbordt, "Active listening room compensation for massive multichannel sound reproduction systems using wave-domain adaptive filtering," J. Acoust. Soc. Am. **122**(1), 354–369 (2007).
[25]L. Fuster, J. J. Lopez, A. Gonzalez, and P. D. Zuccarello, "Room compensation using multichannel inverse filters for wave field synthesis systems," in *Proceedings of the 118th Convention of AES* (May 28–31, 2005).
[26]M. A. Poletti, F. M. Fazi, and P. A. Nelson, "Sound-field reproduction systems using fixed-directivity loudspeakers," J. Acoust. Soc. Am. **127**(6), 3590–3601 (2010).
[27]M. M. Boone and. O. J. Ouweltjes, "Design of a loudspeaker system with a low-frequency cardiodlike radiation pattern," J. Audio Eng. Soc. **45**(9), 702–707 (1997).
[28]W. Anhert and F. Steffen, *Sound reinforcement engineering* (E and FN Spon, London, 1999), pp. 79–125.
[29]R. P. Glover, "A review of cardioid type unidirectional microphones," J. Acoust. Soc. Am. **11**(3), 296–302 (1940).
[30]E. G. Williams, *Fourier Acoustics* (Academic Press, San Deigo, 1999), pp. 183–234, 251–295.
[31]E. Skudrzyk, *The Foundations of Acoustics* (Springer-Verlag, New York, 1971), pp. 344–377.
[32]D. Colton and R. Kress, "Inverse Acoustic and Electromagnetic Scattering Theory," in *Applied Mathematical Sciences*, 2nd ed. (Springer, Berlin, 1998), Vol. 93, pp. 21–28.
[33]S. Spors and J. Ahrens, "A comparison of wave field synthesis and higher-order ambisonics with respect to physical properties and spatial sampling," in *Proceedings of the 125th Convention of AES* (October 2–5, 2008).
[34]http://www.personal.soton.ac.uk/jf1w07/nodes/nodes.html, last accessed March 3, 2010.
[35]G. H. Golub and C. F. Van Loan, *Matrix Computations* (Johns Hopkins University Press, Baltimore, MD, 1983) pp. 136–188.
[36]L. L. Scharf, *Statistical Signal Processing: Detection, Estimation and Time Series Analysis* (Addison-Wesley Publ. Co., Massachusetts, 1991), pp. 359–422.
[37]A. Edelman, "Eigenvalues and condition numbers of random matrices," SIAM J. Matrix Anal., Vol. **9**, No. 4, 543–560 (October 1988).